Journal of Experimental Botany, Vol. 72, No. 10 pp. 3554–3568, 2021
doi:10.1093/jxb/erab094 Advance Access Publication 4 March, 2021

RESEARCH PAPER

Potential interaction between autophagy and auxin during maize leaf senescence

Xue Feng[1,2,*], Lili Liu[1,2,*], Zhigang Li[1,2], Fang Sun[1,2], Xiaoyuan Wu[1], Dongyun Hao[3], Huaiqing Hao[1,†], and Hai-Chun Jing[1,2,4,†],

[1] Key Laboratory of Plant Resources, Institute of Botany, Chinese Academy of Sciences, Beijing, 100093, China;
[2] University of Chinese Academy of Sciences, Beijing, 100049, China;
[3] Institute of Agricultural Biotechnology, Jilin Academy of Agricultural Sciences, Changchun, Jilin 130124, China;
[4] Engineering Laboratory for Grass-based Livestock Husbandry, Institute of Botany, Chinese Academy of Sciences, Beijing, 100093, China

* These authors contributed equally to this work.
† Correspondence: hcjing@ibcas.ac.cn or hqhao@ibcas.ac.cn

Received 15 December 2020; Editorial decision 9 February 2021; Accepted 1 March 2021

Editor: Ariel Vicente, CONICET- National University of La Plata, Argentina

Abstract

Leaf senescence is important for crop yield as delaying it can increase the average yield. In this study, population genetics and transcriptomic profiling were combined to dissect its genetic basis in maize. To do this, the progenies of an elite maize hybrid Jidan27 and its parental lines Si-287 (early senescence) and Si-144 (stay-green), as well as 173 maize inbred lines were used. We identified two novel loci and their candidate genes, *Stg3* (*ZmATG18b*) and *Stg7* (*ZmGH3.8*), which are predicted to be members of autophagy and auxin pathways, respectively. Genomic variations in the promoter regions of these two genes were detected, and four allelic combinations existed in the examined maize inbred lines. The $Stg3^{Si\text{-}144}/Stg7^{Si\text{-}144}$ allelic combination with lower *ZmATG18b* expression and higher *ZmGH3.8* expression could distinctively delay leaf senescence, increase ear weight and the improved hybrid of NIL-$Stg3^{Si\text{-}144}/Stg7^{Si\text{-}144}$ × Si-144 significantly reduced ear weight loss under drought stress, while opposite effects were observed in the $Stg3^{Si\text{-}287}/Stg7^{Si\text{-}287}$ combination with a higher *ZmATG18b* expression and lower *ZmGH3.8* expression. Thus, we identify a potential interaction between autophagy and auxin which could modulate the timing of maize leaf senescence.

Keywords: Autophagy and auxin pathways, interaction, leaf senescence, maize yield, population genetics, transcriptomic profiling.

Introduction

Senescence, an indispensable process for nutrient remobilisation at the final stage of leaf development, plays a crucial role in crop yield (Wu *et al.*, 2012; Thomas and Ougham, 2014). The onset of leaf senescence depends on the developmental stages of a leaf, which are known as age factors or age-related changes (Jing *et al.*, 2003; Schippers, 2015). Leaf senescence can also be induced by various biotic or abiotic stresses, such as pathogen infection, drought stress and darkness (Guo and Gan,

2012; Liang *et al.*, 2014). During leaf senescence, many physiological, biochemical and molecular processes are initiated, such as breakdown of chlorophyll, destruction of photosynthetic membrane systems, changes in source-sink communication, and expression of thousands of senescence-associated genes (*SAG*s), which are generally referred to as the senescence syndrome (Bleecker and Patterson, 1997; Schippers *et al.*, 2015; Yolcu *et al.*, 2018). The timely delaying of senescence or prolonging of stay-green stage are beneficial to extend the leaf functional period, which can facilitate the source strength and thus improve crop yield (Jordan *et al.*, 2012; Gregersen *et al.*, 2013). For example, delaying leaf senescence can increase the average yield by 0.29 tonne ha^{-1} in maize (Zhang *et al.*, 2019), 10% in rice (Mao *et al.*, 2017), and 6–28% in wheat (Christopher *et al.*, 2008). Therefore, it is of great importance to illustrate the underlying molecular mechanisms of leaf senescence for crop breeding.

Maize (*Zea mays*) is one of the most important multi-purpose plants, functioning not only as food, but also as feed, fuel and industrial raw materials. Selection and breeding of stay-green or senescence-delayed cultivars have been considered as one of the effective strategies to tackle the challenges of yield stability caused by the frequent occurrence of climatic disasters, especially drought stress. Inbred lines with distinct leaf senescence differences such as Qi-319, Mo17, Zheng58, CML444 and A150-3-2, have been selected as the parental lines in maize. By using various populations including recombinant inbred lines (Zheng *et al.*, 2009; Messmer *et al.*, 2011; Wang *et al.*, 2012; Almeida *et al.*, 2014; Khanal *et al.*, 2015; Yang *et al.*, 2017), backcrossed lines (Belícuas *et al.*, 2014; Trachsel *et al.*, 2016), topcross progenies (Beavis *et al.*, 1994) and double haploids (Liu *et al.*, 2020), a total of 268 major quantitative trait loci (QTL) for this trait have been mapped onto the 10 chromosomes, accounting for 0.5–24.3% of phenotypic variation. In addition, transcriptomic analyses have identified a large number of differentially expressed genes (DEGs) for leaf senescence in maize, which are significantly enriched in hormone biosynthesis, photosynthesis, carbohydrate metabolism and amino acid transport (Sekhon *et al.*, 2012; Zhang *et al.*, 2014; Chai *et al.*, 2019; Sekhon *et al.*, 2019).

However, so far, only a small number of genes controlling leaf senescence have been characterised at the molecular or cellular level in maize. Some of them were characterised by reverse genetic approaches. For instance, ACC (aminocyclopropane-1-carboxylic acid) synthases (ACS) are the enzymes at the first step of ethylene biosynthesis, and the *Mu*-insertion lines of *ACS6* in maize showed a reduction in ethylene synthesis and delayed leaf senescence (Young *et al.*, 2004). *ZmVQ52* is a VQ family transcription factor (proteins containing a unique and conserved VQ motif). Overexpression of *ZmVQ52* in Arabidopsis showed premature leaf senescence, and the transcriptomic data revealed that this function was mainly through photosynthesis and circadian rhythm pathways. Additionally, the overexpression lines exhibited enhanced sensitivities to jasmonic acid (JA) and salicylic acid (SA), but were tolerant to abscisic acid (ABA), suggesting a potential connection between ZmVQ52 and hormone signalling in the regulation of leaf senescence (Yu *et al.*, 2019). *SnRK1s* (sucrose non-fermenting-1-related protein kinase 1 genes) encode enzymes that are important members in sugar signalling and carbohydrate metabolism, and the ectopic expression of *ZmSnRK1* in Arabidopsis distinctly delayed leaf senescence, suggesting that *ZmSnRK1* may have a similar function in maize (Wang *et al.*, 2019). Furthermore, some genes have been identified by forward genetic approaches. Through genome-wide association study (GWAS), two genes were analysed. *Mir3* encodes a cysteine protease, and the knockout mutant of its ortholog *RD21A* in Arabidopsis exhibited loss of protease activity and a delayed leaf senescence phenotype. In the senescent line, an earlier onset of β-glucosidase activity was detected, while the stay-green line showed a delayed β-glucosidase activity, potentially caused by the differential post-transcriptional regulation of *BGLU42* (β-gluosidase-42; Sekhon *et al.*, 2019). By QTL mapping, a gene encoding a NAC [No apical meristem (NAM), Arabidopsis transcription activation factor (ATAF) and cup-shaped cotyledon (CUC)]-domain transcription factor, named *NAC7,* was characterised. RNA-sequencing (RNA-seq) analysis revealed that genes encoding photosynthesis-associated enzymes exhibited higher expression but those for chlorophyll degradation showed lower expression in *nac*7 RNAi lines; these enzymes are associated with a delayed leaf senescence phenotype and increased grain yield, demonstrating that NAC7 acts as a negative regulator of photosynthetic activities, promotes chlorophyll degradation, and accelerates leaf senescence (Zhang *et al.*, 2019). Recently, a transcriptomic analysis reported that ZmNAC126 was a positive regulator in chlorophyll degradation by affecting the expression of *CCG*s (*CHLOROPHYLL CATABOLIC GENES*) to promote leaf senescence. Meanwhile, expression of *ZmNAC126* was up-regulated in response to ethylene treatment, which accelerated leaf senescence in maize, suggesting the molecular link between chlorophyll degradation and ethylene pathway (Yang *et al.*, 2020).

Information from breeders revealed that Jidan27 is an elite maize hybrid, which is specifically bred for North-eastern China Corn Belt with cumulative temperatures between 2300–2500 °C in Heilongjiang Province. The hybrid usually suffers from premature leaf senescence at the adult plant stage, presumably from the female parent Si-287, which displays a prominently accelerated senescence phenotype compared with the male parent Si-144. In-depth investigation of leaf senescence will facilitate targeted maize improvement.

Here, through an integrated analysis of population genetics and transcriptome profiling, we identified two candidate genes, *ZmATG18b* and *ZmGH3.8*, which are important components in autophagy and auxin pathways, respectively. Four combinations were found for the natural allelic variations of these two genes in maize inbred lines. The subtle balance between their expression in different allelic combinations is closely related

to leaf senescence and yield trait, indicating that the potential interaction between autophagy and auxin at a transcriptional level might be involved in regulating the timing of maize leaf senescence.

Materials and methods

Plant materials and field experiments

Two maize inbred lines, Si-287 and Si-144 with distinctive senescence phenotypes were obtained from Jilin Academy of Agricultural Sciences (Changchun, China). Si-287 (carrying $Stg3^{Si\text{-}287}/Stg7^{Si\text{-}287}$ alleles) is derived from a cross between the maize inbred line 444 and Jin-03, and Si-144 (carrying $Stg3^{Si\text{-}144}/Stg7^{Si\text{-}144}$ alleles) is derived from a Thai hybrid.

An F_2 population with 207 individuals was developed from a cross between Si-287 (female parent) and Si-144 (male parent). Moreover, 3725 individual plants of BC_3F_2, BC_3F_3 and BC_3F_4 generations were generated from repetitive back-crossed progeny from a cross between Si-287 (recipient) and F_2 individuals (donor). The near-isogenic lines (NILs), which contained one [NIL-$Stg3^{Si\text{-}144}$ (carrying $Stg3^{Si\text{-}144}/Stg7^{Si\text{-}287}$ alleles), NIL-$Stg7^{Si\text{-}144}$ (carrying $Stg3^{Si\text{-}287}/Stg7^{Si\text{-}144}$ alleles)] or two [NIL-$Stg3^{Si\text{-}144}/Stg7^{Si\text{-}144}$ (carrying $Stg3^{Si\text{-}144}/Stg7^{Si\text{-}144}$ alleles)] donor segments, were screened from the progeny in the BC_3F_4 generation. In addition, a total of 173 maize inbred lines collected from Jilin Academy of Agricultural Sciences (Changchun, China) were used in this study (Supplementary Table S1).

During the natural growing season, maize plants were planted in the experimental fields in Beijing, China (39°55' N, 116°18' E) in 2015 and 2016, Sanya, Hainan Province, China (18°36' N, 108°42' E) in 2016, and Jinta, Gansu Province, China (39°57' N, 98°22' E) in 2018 and 2019. Plant materials were grown in the normal conditions in accordance with the local agriculture practices. In the summer of 2017, the improved hybrids and Jidan27 (as hybrid control) for drought tolerance analysis were grown at the experimental fields in Jinta, Gansu Province and Bayan Nur, Inner Mongolia, China (40°75' N, 107°42' E), respectively. These two locations are all with low annual rainfall and large evaporation during the growth period. For the well-watered conditions, the management followed the local agricultural practices. For the drought stress conditions, water was withheld from seven days days before anthesis (DBA) to 45 days after anthesis (DAA), and other management was the same as the well-watered conditions.

Phenotypic data collection

The maize population varied substantially in flowering time, spanning from 68 to 110 days after sowing. To accurately record and calculate the phenotype of leaf senescence, we firstly marked the fifth and tenth leaves of five randomly selected plants with red paint at seedling stage and V10 stage (when the tenth leaf is fully unfolded). The date was then recorded when more than half of the plants were flowering for each line and was counted as day 0. The number of leaves (LN) was also recorded. We divided the yellowing degree of maize leaves (YDL) into five grades: 0, 25%, 50%, 75%, and 100%, and recorded this trait at day zero and on day 30. Then the percentage of green leaves (PGL) was calculated following the formula: PGL =1− (Total YDL)/LN. For the improved hybrid lines, the reduction of the percentage of green leaves = $[(PGL_{WW} - PGL_{DS})/PGL_{WW}] \times 100\%$, $_{WW}$ represents well-watered condition, and $_{DS}$ represents drought stress condition. The optimal photochemical efficiency of PSII (*Fv/Fm;* Maxwell and Johnson, 2000; Bresson *et al.*, 2018) was measured after 2 h of dark adaption using a closed FluorCam instrument (Photon Systems Instruments, Czech Republic). After harvesting, ear weight of maize inbred lines was measured with at least three plants per line, and those of the improved hybrids and Jidan27 were measured with at least eight plants from each kind.

Chlorophyll measurement

Chlorophyll of the collected samples was extracted using 80% (v/v) acetone at 25–26 °C for 24 h in the dark. Before quantification, the mixture was centrifuged at 6000 × *g* for 10 min. The absorbance of the supernatant was measured at 645 nm and 663 nm, and total chlorophyll content was calculated by the formula: C_t (mg l^{-1}) = 20.2 ×A_{645}+8.02 ×A_{663}, and the volume of extracted solution and the fresh weights of tissues were used to calculate the concentration of chlorophyll in leaves (Arnon, 1949).

Soluble protein measurement

Plant materials were extracted in double-distilled water. The mixture was centrifuged at 5000 × *g* for 10 min at 4 °C. Then the supernatant was collected, after which 100 µl of the collected supernatant was taken, and 900 µl double distilled water and 5 ml Coomassie brilliant blue G250 were added for mixing [for the standard curve, supernatant and double distilled water were replaced by Bovine serum albumin (BSA) standard solution of different concentrations]. After 2 min standing, the absorbance at 595 nm was measured. The soluble protein concentration of different samples was calculated according to the equation (C × Vt) / (FW × Vs ×1000). C represents the value from a standard curve, Vt and Vs represent the volume of extracted solution and the volume of test solution, respectively, and FW represents the fresh weight of leaf samples.

RNA extraction and RT–qPCR analysis

Leaf samples were collected in the field at seven DBA and 30 DAA, then quickly frozen in liquid nitrogen and stored at −80°C for RNA extraction. Three biological replicates were carried out for each sample. Total RNA was extracted by Quick RNA isolation Kit [Huayueyang Biotechnology (Beijing) Co. Ltd., China] and treated with RNase-free DNase I to remove residual genomic DNA, following which $OD_{260/280}$ of the extracted RNA was measured. A ReverTra Ace reverse transcriptase kit (Toyobo, Japan) was used to synthesize cDNA. RT–qPCR analysis was performed with an Eco system (Illumina, USA) using UltraSYBR Mixture (Cwbio, China), and at least three replicates were performed for each sample. After stability evaluation of six candidate reference genes under all experimental conditions by NormFinder and geNorm software tools (Andersen *et al.*, 2004; Vandesompele *et al.*, 2002), *Zm00001d036201*, which encodes a hypothetical protein, was used as the internal control for normalization of gene expression values (Lin *et al.*, 2014; Bertels *et al.*, 2020; (Supplementary Fig. S1). The relative expression of amplified genes was calculated by the $2^{-\Delta\Delta Ct}$ method (Livak and Schmittgen, 2001). Primers used for RT–qPCR analysis are listed in Supplementary Table S2. Detailed information about RT–qPCR is listed in Supplementary Table S3 (Bustin *et al.*, 2009).

Molecular marker development and genotyping

Genomic DNA of each individual was extracted by the CTAB method (Murray and Thompson, 1980; Causse *et al.*, 1994). Kompetitive Allele-Specific PCR (KASP) markers were developed [China Golden Marker (Beijing) Biotech Co., Ltd., China] on the basis of the B73 genome, and a total of 127 markers were used after validation in Si-287 and Si-144. In addition, the InDel and SNP (single nucleotide polymorphism) markers were developed for fine mapping of the target loci. Primers were designed with the Primer Premier 5.0 software. The polymorphisms of designed markers were screened between the parental lines using agarose gel electrophoresis or Sanger sequencing. All the molecular markers developed for genotyping are listed in Supplementary Table S4.

Classical QTL mapping and QTL-seq analysis

QTL analysis of the F_2 population was conducted using the QTL IciMapping software (version 4.1) via inclusive composite interval mapping (ICIM-ADD; Meng *et al.*, 2015). The threshold of LOD (logarithm of odds) for a quantitative trait locus was determined by 1000 permutation tests at a significance level of P=0.05, and the additive effects were also displayed.

QTL-seq approach (whole-genome sequencing-based QTL mapping; Takagi *et al.*, 2013) was performed in the BC_3F_2 population. Two bulked DNA pools with extreme phenotypes (stay-green pool, C2 and senescence pool, C1) were prepared by mixing DNA from 30 individuals in an equal ratio. Furthermore, whole-genome resequencing of the selected DNAs was carried out, and the high-quality reads obtained from the DNA bulks were aligned to the reference sequence to identify SNPs (Supplementary Table S5). SNP-index was calculated for all the detected SNP positions, and those with sequencing depth <7 and SNP-index <0.3 were excluded from the two extreme bulks. After filtering, 4 817 475 SNPs were obtained, and Δ(SNP-index) was calculated for all these positions by the following formula: Δ(SNP-index) = SNP-index (C2) – SNP-index (C1). With 10 000 replications of the permutation test, the threshold values were selected at the 95% and 99% levels. The candidate loci were obtained in the continuous and evenly distributed regions that exceeded the 99% confidence threshold. Furthermore, recombinant individuals were screened from the successive generations of BC_3F_3 and BC_3F_4 (1106 individuals) with senescent phenotype segregation.

Transcriptome data analysis

Clean reads were obtained by filtering the raw reads (removing the adapters and low-quality sequences) and then mapped to the B73 reference genome (ftp://ftp.ensemblgenomes.org/pub/plants/release-39/fasta/zea_mays/). The HISAT2 software (Version 2.1.0) was used to count the total mapped reads and uniquely mapped rate (Kim *et al.*, 2015). FPKM (Fragments Per Kilobases per Millionreads) values were used to calculate gene expression with RSEM software (Version 1.2.31; Li and Dewey, 2011). DEGs were obtained by DEseq2 software (Version 1.22.1; Love *et al.*, 2014) with the condition of $|\log_2(\text{fold change})| \geq 1$, FDR <0.05 (false discovery rate). Gene clustering and pathway enrichment were conducted by R (Version 3.5.3).

Sequence analysis and natural variations of the candidate genes

Genomic sequences of the candidate genes were amplified from Si-287 and Si-144 by KOD-Plus-Neo (Toyobo, China). Primers used for the amplification are listed in Supplementary Table S6. PCR was performed in a 25 μl volume containing 2.5 μl 10 × PCR buffer, 2.5 μl dNTPs (2 mM), 1.5 μl $MgSO_4$ (25 mM), 1 μl forward primer (10 μM) and 1 μl reverse primer (10 μM), 1 μl DNA template (100 ng μl^{-1}), 0.5 μl KOD-Plus-Neo (1 U μl^{-1}) and 15 μl sterile water. All the amplifications were carried out on an Applied Biosystems Veriti Thermal Cycler (ABI, USA), and the cycling program was 94 °C for 2 min, followed by 38 cycles at 98 °C for 10 s, 58 °C for 30 s and 68 °C for 1–2 min 30 s, then an extension at 68 °C for 7 min. The PCR products were separated and purified by a 1.5% agarose gel, and the DNA was extracted from the fragments and sequenced by Sanger sequencing. The alignments of the obtained sequences were conducted by DNAMAN software (version 7.0), and variations between the parental lines were detected. The gene structure in this study was drawn by IBS software (Liu *et al.*, 2015).

Natural variations of the candidate genes were amplified from 173 maize inbred lines by PCR using Goldstar Best MasterMix (Cwbio). The genotype of each line was distinguished by agarose gel electrophoresis or sequenced by Sanger sequencing, and aligned to identify variations.

Results

Allelic variation at two major QTL from the parental lines of an elite maize hybrid differentially contribute to leaf senescence

A detailed characterisation of the differences in leaf senescence between Si-287 and Si-144 was carried out in the field. We mainly focused on the senescence phenotypes of the ear leaves and the whole plant. No differences were observed prior to 30 days after anthesis (DAA); thereafter, an obvious yellowing of the ear leaves occurred in Si-287, whereas those of Si-144 remained green (Fig. 1A), and the percentage of green leaves of the two lines were 52% and 97%, respectively (Fig. 1B). Consistent with the differences in visual phenotype, the concentration of chlorophyll and soluble proteins in Si-287 were significantly (P<0.01)lower than those in Si-144 (Fig. 1C, D). Two marker genes (*ZmNYE1-like* and *ZmNAC7*) that participate in chlorophyll degradation in maize leaf senescence were more highly expressed in Si-287 than in Si-144 (Fig. 1E, F). At 45 DAA, Si-287 and Si-144 exhibited distinct differences in the whole plant senescence, and the percentage of green leaves further dropped to 5% and 72%, respectively (Fig. 1G). Thus, these two lines differed substantially in their ageing characteristics.

To dissect the genetic loci controlling leaf senescence in these two maize lines, we first constructed a segregating population by a cross between Si-287 and Si-144 (Fig. 2A), and scored the percentage of the yellow leaves in an F_2 population consisting of 207 individuals at 30 DAA. We found that the leaf senescence trait was continuous and followed a normal distribution pattern (Fig. 2B). A total of 101 polymorphic KASP markers between the parental lines distributed across the 10 chromosomes in maize were further used to genotype the F_2 individuals. The two sets of data were input into the QTL IciMapping software for QTL analysis, and three major loci were detected on chromosomes (Chr) 3, 7, and 8 (Supplementary Table S7), which were designated as *Stg3*, *Stg7*, and *Stg8*, and the phenotypic variation explained (PVE) was 7.4% (LOD =3.40), 8.41% (LOD =4.04) and 6.62% (LOD =3.40), respectively. The additive effects of *Stg3* and *Stg7* were both positive, indicating that the alleles derived from Si-287 had enhanced effects on leaf senescence (Z. Zhang *et al.*, 2016). In comparison with *Stg3* and *Stg7*, the additive effects of *Stg8* was negative (–0.05), and hence alleles from Si-287 contributed to the delay of the leaf senescence phenotype. Here, we primarily focused on *Stg3* and *Stg7,* which are more relevant to breeding applications. We then selected stay-green (non-senescent) lines to successive back-crosses with Si-287 to further construct the back-cross population. The corresponding alleles in Si-287 and Si-144 were named as $Stg3^{Si\text{-}287}/Stg7^{Si\text{-}287}$ and $Stg3^{Si\text{-}144}/Stg7^{Si\text{-}144}$, respectively.

The BC_3F_2 population was obtained from the self-pollination of selected individuals in the BC_3F_1 generation (Fig. 2A),

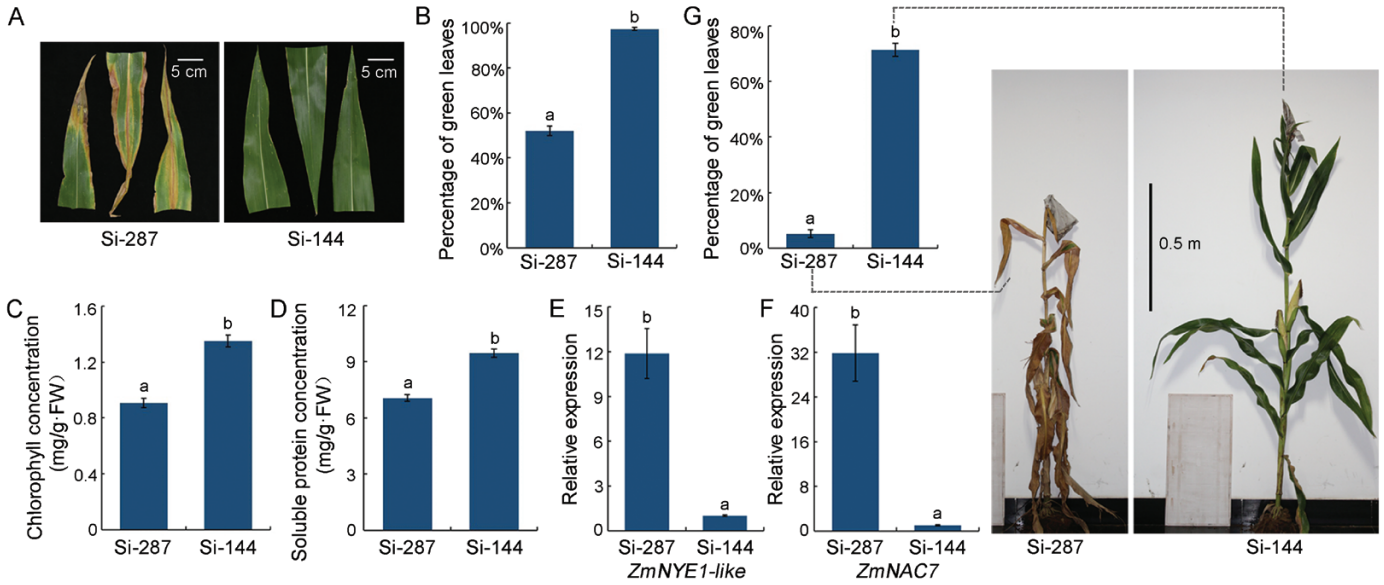

Fig. 1. Contrasting phenotypes of leaf senescence between two parental lines. (A) Senescence phenotypes of ear leaves between inbred lines Si-287 and Si-144. Scale bar =5 cm. (B) Statistical analysis of green leaves ratio in (A). (C, D) Bar charts of the concentration of chlorophyll (C) and soluble protein (D) in the parental lines Si-287 and Si-144. (E, F) Expression patterns of the senescent marker genes *ZmNYE1-like* (E) and *ZmNAC7* (F) in Si-287 and Si-144, determined by RT-qPCR. (G) Leaf senescence phenotypes of Si-287 and Si-144 at the whole plant level at 45 DAA. Scale bar =0.5 m. Bar chart shows the ratio of green leaves. Samples analysed in (A-F) are Si-287 and Si-144 collected at 30 DAA. Different letters above the bar charts indicate differences at the 0.05 significance level determined by two-tailed Student's *t* test.

and leaf senescence phenotypes of 1904 plants were measured. To confirm the loci (*Stg3* and *Stg7*) detected by the classical QTL mapping, a QTL-seq approach which is based on next-generation sequencing (NGS) technology and widely used in many plant species (Takagi *et al.*, 2013; Lu *et al.*, 2014; Zheng *et al.*, 2020), was performed on respective 30 individuals with extreme phenotypes (senescence and stay-green). At the 99% level of significance, two major QTL were detected on Chr3 (145.66–161.01 Mb) and Chr7 (167.12–170.68 Mb), which overlapped with the major regions of *Stg3* and *Stg7*, respectively, identified by classical QTL mapping (Fig. 2C, D). To further narrow down the targeted intervals, 30 pairs of polymorphic molecular markers were developed to dissect the BC_3F_3 and BC_3F_4 populations (Supplementary Table S4), and 1106 individuals were genotyped (Fig. 2A). Finally, *Stg3* was mapped to a 5.86 Mb interval, and *Stg7* to a 380 kb interval (Fig. 2C, D). These data suggest that these two loci might play vital roles in delaying leaf senescence, and genes in the targeted regions deserve further analysis.

To validate the function of *Stg3* and *Stg7*, we identified the background of homozygous recombinants from the BC_3F_4 population, and a total of six individuals possessing the *Stg3* [NIL-$Stg3^{Si\text{-}144}$ (carrying $Stg3^{Si\text{-}144}/Stg7^{Si\text{-}287}$ alleles)], *Stg7* [NIL-$Stg7^{Si\text{-}144}$ (carrying $Stg3^{Si\text{-}287}/Stg7^{Si\text{-}144}$ alleles)] and both the two loci [NIL-$Stg3^{Si\text{-}144}/Stg7^{Si\text{-}144}$ (carrying $Stg3^{Si\text{-}144}/Stg7^{Si\text{-}144}$ alleles)] from the donor parent (Si-144) were selected (Supplementary Fig. S2). The genetic background recovery rates of all these NILs ranged from 90.4% to 98.1% (Supplementary Table S8). To further determine the function of these two major loci, the characteristics of leaf senescence were analysed. Compared with Si-287, which was senescent at 30 DAA, delayed leaf senescence was observed in all the NILs (Supplementary Fig. S3A), as shown by the significantly ($P<0.05$) higher percentage of green leaves and the concentration of chlorophyll in NILs compared with those in Si-287 (Fig. 3A, B). Soluble protein concentrations in NIL-$Stg7^{Si\text{-}144}$ was higher than that in Si-287, but no significant difference ($P>0.05$) was detected amongst NIL-$Stg3^{Si\text{-}144}$, NIL-$Stg3^{Si\text{-}144}/Stg7^{Si\text{-}144}$ and Si-287 (Fig. 3C). We further measured the *Fv/Fm* values of different lines and found that the photosynthetic activity of Si-287 was significantly ($P<0.01$) lower than that of NILs (Supplementary Fig. S3B; Fig. 3D). At 45 DAA, significant ($P<0.01$) phenotypic differences were observed between Si-287 and NILs. Si-287 was almost completely yellow, while NILs remained green and the percentage of green leaves was significantly ($P<0.01$) higher than that of Si-287 (Fig. 3E, F).

SAGs *contributing to phenotypic variation of leaf senescence identified by transcriptomic analysis*

Leaf senescence is driven by thousands of so-called *SAG*s. To understand the differences in leaf senescence in the parental lines at the transcriptional level, we performed RNA-seq analysis of Si-287 and Si-144. Raw data were acquired with Q30 >95%, and 596 490 046 reads were obtained after filtering and quality control (Supplementary Table S9). Here, we mainly focused on the unique up-regulated genes in Si-287 and those shared by Si-287 and Si-144 with $|\Delta FC| \geq 2$. Therefore, a three-step data analysis protocol was used to further identify *SAG*s: (i) by

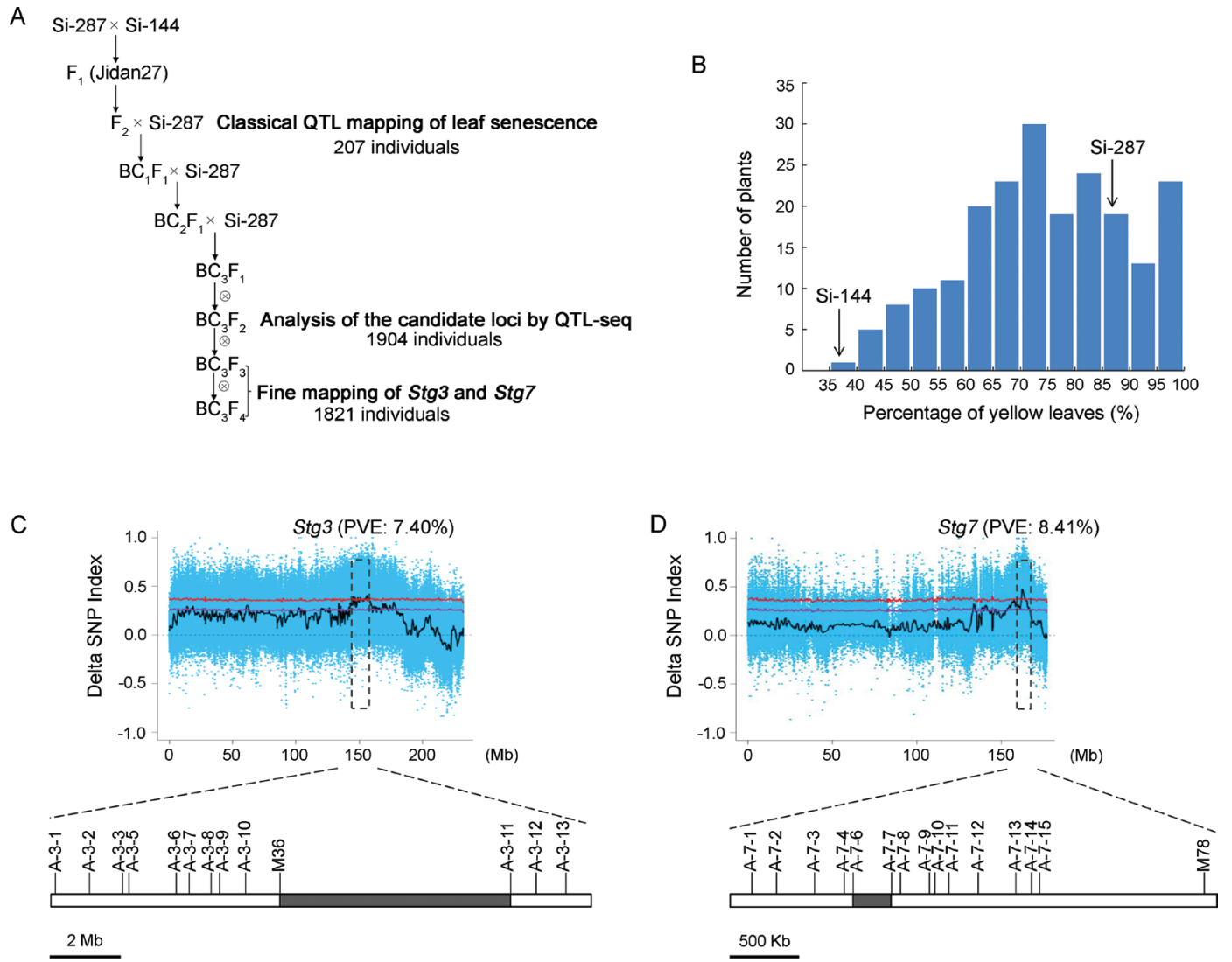

Fig. 2. Identification of two major loci for leaf senescence via QTL mapping. (A) The scheme of the construction of mapping population for the detection of candidate loci controlling leaf senescence. Si-287 was used as the recurrent parent backcrossed for three generations. (B) Frequency distribution of leaf senescence in F_2 population. (C) Identification of leaf senescence locus *Stg3* on Chr3. PVE represents phenotypic variation identified from classical QTL mapping in F_2 population. Delta SNP Index graph from QTL-seq further identified *Stg3* in the region of 145.66–161.01 Mb on Chr3. Linkage analysis with molecular markers on the mapping population delimited the region to an interval between markers M36 and A-3–11. (D) Identification of leaf senescence locus *Stg7* on Chr7. Delta SNP Index graph from QTL-seq further identified *Stg7* in the region of 167.12–170.68 Mb on Chr7. Linkage analysis with molecular markers on the mapping population refined the location to an interval defined by molecular markers A-7-6 and A-7-7.

comparing the gene expression at 30 DAA with seven DBA, DEGs of Si-287 and Si-144 were detected. A total of 3577 up-regulated and 1424 down-regulated genes were identified in Si-287, and 3958 up-regulated and 1824 down-regulated genes were identified in Si-144 (Fig. 4A); (ii) we then compared the up-regulated genes between Si-287 and Si-144, and removed DEGs between Si-287_7 DBA and Si-144_7 DBA to avoid the effects of developmental stages and genetic background (Fig. 4B), because the phenotype of leaf senescence was not different between Si-287 and Si-144 at the initial stage (7 DBA). Then we obtained 1671 specific up-regulated DEGs in Si-287 (Fig. 4B); (iii) genes in the shared part between Si-287 and Si-144 in the up-regulated DEGs were also important for us to detect *SAG*s. Amongst them, the 461 genes in U2 set with $|\Delta FC| \geq 2$ were of more interest to us (Fig. 4B). Finally, we obtained the *SAG*s set of 2132 genes, including 1671 up-regulated DEGs and 461 genes in U2 set with $|\Delta FC| \geq 2$ (Fig. 4B). We further compared our results (*SAG*s_Si-287) with a previous transcriptome study (*SAG*s_B73) of maize developmental leaf senescence (Sekhon *et al.*, 2019). Although different plant materials were used (Si-287 and B73), 1655 common genes were still identified. Gene ontology (GO) enrichment analysis revealed that these common genes were significantly enriched in sugar catabolism, autophagy, amino acid

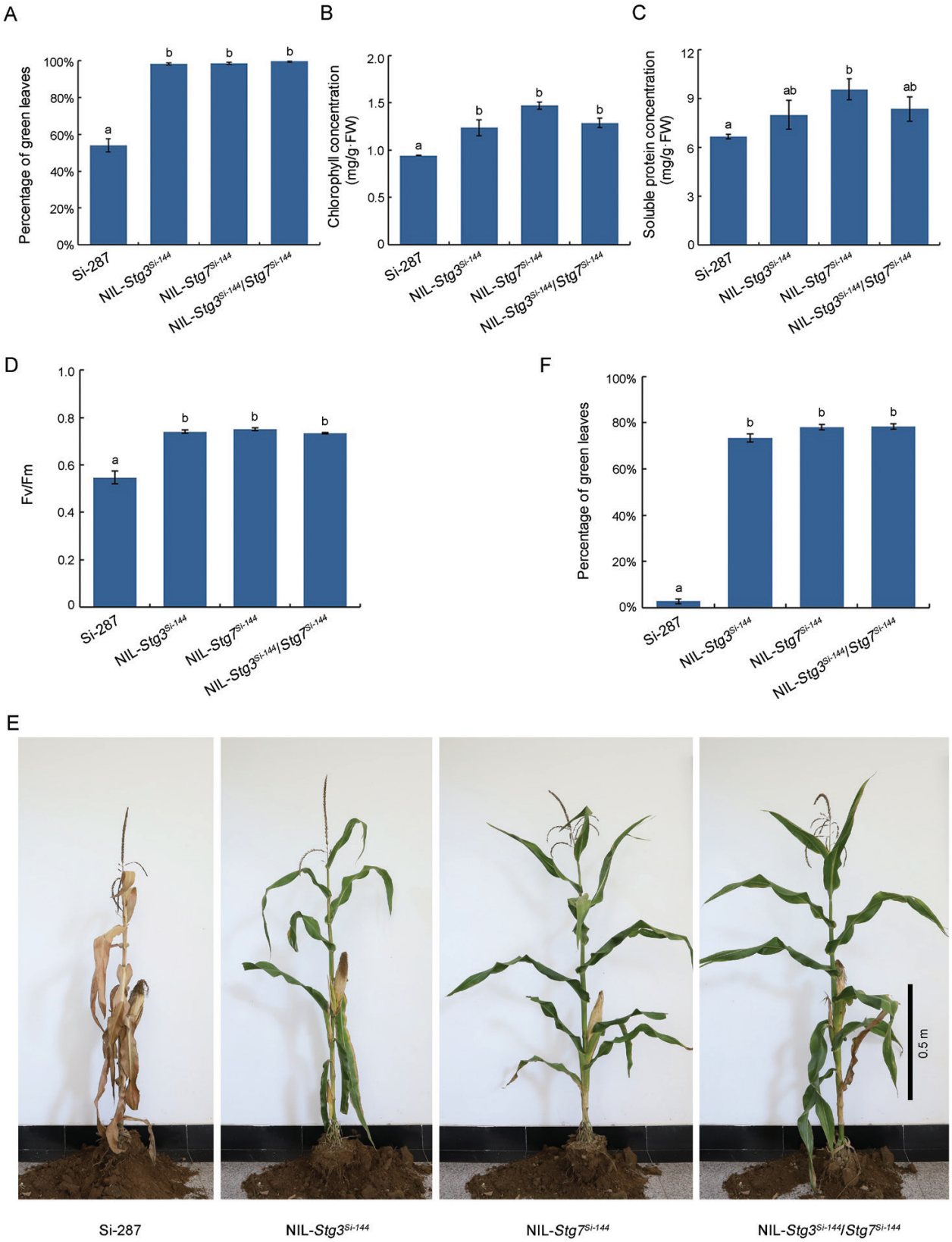

Fig. 3. Alleles of *Stg3*$^{Si\text{-}144}$ and *Stg7*$^{Si\text{-}144}$ delayed leaf senescence. (A) Statistic analysis of green leaves ratio of Si-287 and NILs (NIL-*Stg3*$^{Si\text{-}144}$, NIL-*Stg7*$^{Si\text{-}144}$ and NIL-*Stg3*$^{Si\text{-}144}$/*Stg7*$^{Si\text{-}144}$). Si-287 harboured the combination of alleles of *Stg3*$^{Si\text{-}287}$*Stg3*$^{Si\text{-}287}$/*Stg7*$^{Si\text{-}287}$*Stg7*$^{Si\text{-}287}$. NIL-*Stg3*$^{Si\text{-}144}$ = near-isogenic line with the *Stg3*$^{Si\text{-}144}$ allele in Si-287 background; NIL-*Stg7*$^{Si\text{-}144}$ = near-isogenic line with the *Stg7*$^{Si\text{-}144}$ allele in Si-287 background; NIL-*Stg3*$^{Si\text{-}144}$/*Stg7*$^{Si\text{-}144}$ = near-isogenic line with the stacking of *Stg3*$^{Si\text{-}144}$ allele and *Stg7*$^{Si\text{-}144}$ allele in Si-287 background. (B, C) Concentration of

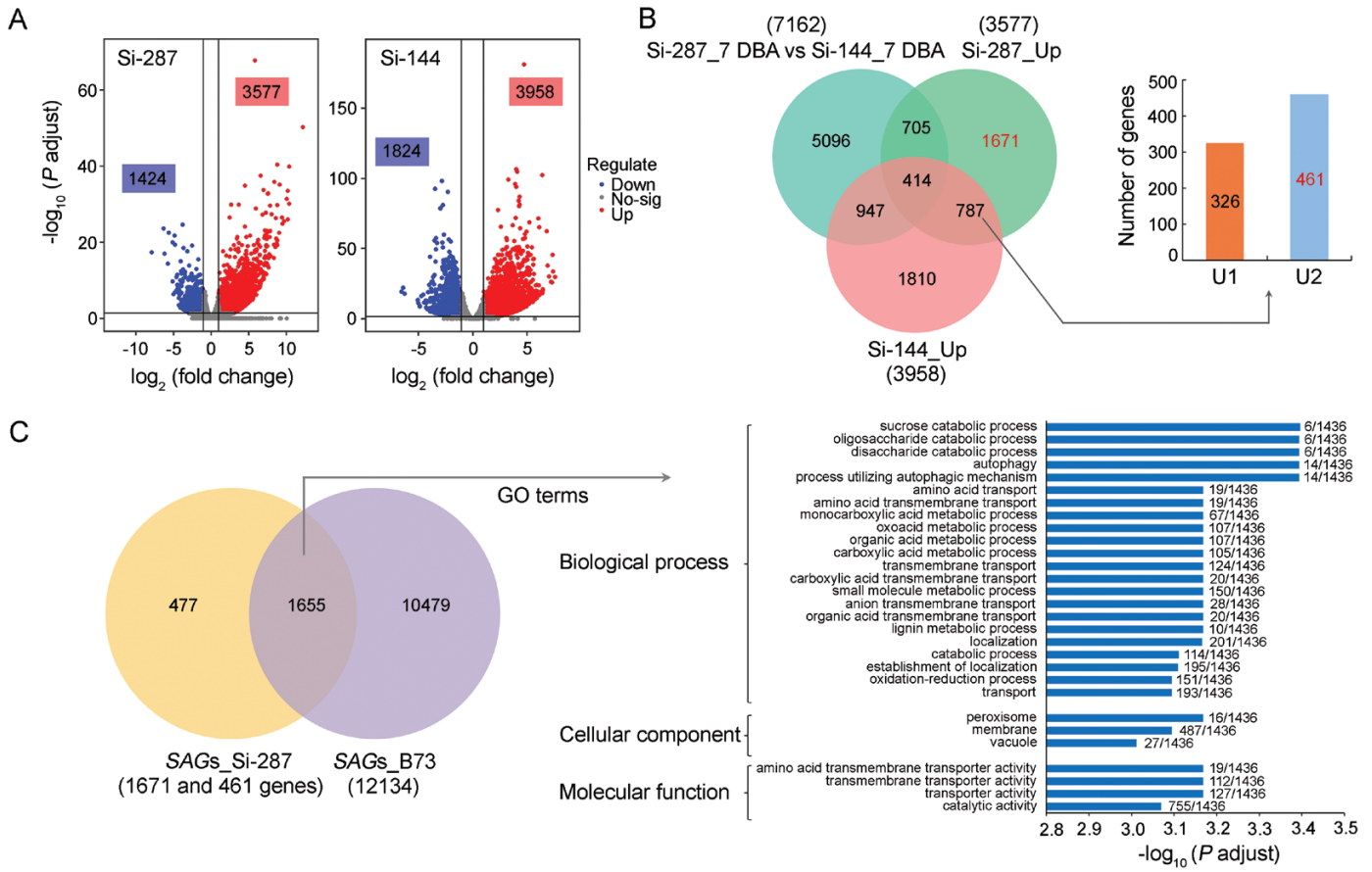

Fig. 4. *SAGs* identified by transcriptome analysis of the parental lines. (A) DEGs in Si-287 and Si-144 were obtained from the comparison of gene expression between 30 DAA and 7 DBA [|$\log_2$(fold change)| ≥1, FDR <0.05], respectively. The blue colour represents down-regulated genes, and the red colour represents up-regulated genes. (B) The identification of *SAGs*_Si-287 set including 1671 genes and 461 genes. The comparison was conducted between Si-287_Up set (3577 genes) and Si-144_Up set (3958 genes), and genes in Si-287_7 DBA versus Si-144_7 DBA set were excluded, then 1671 genes which were unique in Si-287_Up were obtained. In addition, 787 common genes in Si-287_Up and Si-144_Up were divided into two respective sets, including U1 set with 326 genes and U2 set with 461 genes. Genes in U1 set represent their differences in fold change between Si-287 and Si-144 that were less than two (|ΔFC| <2), while genes in U2 set represent their differences in fold change between Si-287 and Si-144 that were greater than or equal to two (|ΔFC|≥2), which were also the candidate *SAGs* in this study. (C) Comparison of genes in the two gene sets, including *SAGs*_Si-287 set identified in this study and a set of DEGs (*SAGs*_B73) in a previous study in maize (Sekhon *et al.*, 2019), and GO categories of 1655 genes in the common region of *SAGs*_Si-287 set and *SAGs*_B73 set. *SAGs*_Si-287 set represents *SAGs* set with 2132 genes in this study, *SAGs*_B73 set represents 12 134 DEGs in Sekhon *et al.* (2019). Numbers on the right side of the columns represent gene numbers in the 1655 gene set enriched for the GO category/the total number of genes in 1655 gene set with GO annotations. Numbers near the Venn labels indicate the total numbers of the key parts.

transport, nutrient transport and catalytic activity categories (Fig. 4C). These results indicate that the identified *SAGs*, especially the 1655 common genes and related GO categories, might be significant regulators of maize leaf senescence.

Putative genes in Stg3 *and* Stg7

Through QTL analysis, we obtained 108 and 13 candidate genes in *Stg3* and *Stg7*, respectively (Supplementary Tables S10; S11). Compared with the *SAGs* set from the transcriptome analysis, three genes were identified. Amongst them, *Zm00001d042215* and *Zm00001d042241* were the candidate genes for *Stg3*. For *Zm00001d042215*, the expression was significantly (P<0.01) higher in Si-287 than that in Si-144 at 30 DAA. However, there was no significant difference (P>0.05) in the expression of *Zm00001d042241* between the parental lines at 30 DAA. Moreover, candidate region association analysis detected a significant SNP [$-\log_{10}$ (P) > 4.63] in *Zm00001d042215*, while no significant [$-\log_{10}$ (P)<4.63] signal was detected in *Zm00001d042241* (Supplementary Fig. S4). Therefore,

chlorophyll (B) and soluble protein (C) of ear leaves in Si-287 and NILs at 30 DAA. (D) Comparison of photosynthesis efficiency (*Fv*/*Fm*) of ear leaves between Si-287 and NILs at 30 DAA. (E) and (F) Senescence phenotypes of Si-287 and NILs at the whole plant level at 45 DAA. Values in (A), (B), (C), (D) and (F) are mean ±SE of three biological replicates. Letters above the columns represent differences at the 0.05 significance level determined by one-way ANOVA.

Zm00001d042215 was selected as the causal gene for *Stg3*. For *Stg7*, *Zm00001d022017* was the only candidate gene (Fig. 5A, B). Furthermore, we analysed the functional annotations of these two genes. *Zm00001d042215* (also named *ZmATG18b*) participates in the formation of autophagosomes and plays a vital role in the autophagy pathway (Li *et al.*, 2015). *Zm00001d022017* (*ZmGH3.8*) encodes an indole-3-acetic acid-amido synthetase (*GH3*) which is involved in auxin metabolism (Du *et al.*, 2012). It deserves attention that both autophagy and auxin pathways have been reported to be involved in plant development and stress responses (Du *et al.*, 2012; Ustun *et al.*, 2017). Thus, we speculated that these two pathways were significant components in maize leaf senescence. To validate this, we analysed the related genes in these two pathways, which fit at least one of the following criteria: (i) genes in the *SAG*s set identified in this study; (ii) genes in both the reported leaf senescence QTL in maize (Zheng *et al.*, 2009; Almeida *et al.*, 2014; Belícuas *et al.*, 2014; Khanal *et al.*, 2015; Trachsel *et al.*, 2016; Yang *et al.*, 2017) and DEGs identified by transcriptome analysis in this study (Fig. 5C). In the main auxin biosynthesis pathway, two genes, *ZmGH3.8* and *ZmYUC5* (*Zm00001d019527*) were found. In the autophagy pathway, a total of 14 genes met the criteria.

Through Sanger sequencing and sequence alignment, we detected the genomic variations of *ZmATG18b* and *ZmGH3.8* between Si-287 and Si-144 (Fig. 5D, E). For *ZmATG18b*, a 6106 bp DNA fragment containing the whole genomic region and the 1600 bp upstream region of 5'UTR were amplified and sequenced. In the genomic region, there was only one variation (A to G) in the first exon, which caused a non-synonymous mutation, but it was not located in the vital motifs of this gene. Considering the differences in expression mentioned above, we compared the variations in the promoter region. A total of 52 variations including SNPs and InDels were detected, two of which were detected in major *cis*-elements (TATA-box and AE-box), which are important elements in stress and light responses. Compared with Si-144, there was a deletion of the TATA-box at −1498 bp (1498 bp upstream of the 5'UTR region) in Si-287. Mutation of A to C was also found in the AE-box at −1439 bp (1439 bp upstream of the 5'UTR region) in Si-287. Thus, the corresponding alleles were designated as $Stg3^{Si\text{-}287}$ type (senescent allele) and $Stg3^{Si\text{-}144}$ type (stay-green or non-senescent allele), respectively (Fig. 5D). For *ZmGH3.8*, 16 and 31 variations were exhibited in the whole genomic region (2492 bp) and the 1600 bp region upstream of 5'UTR, respectively. Amongst them, only two variations existed in the exons, which caused non-synonymous mutations, but they were also not located in the important motifs. Similarly, we speculated that variations in the promoter region might be the causative sites responsible for phenotype differences in leaf senescence. To validate this speculation, we analysed the *cis*-elements in the promoter region, as several auxin-responsive *cis*-elements, such as ARFAT, ASF1MOTIFCAMV (TGACG) and AUXREPSIAA4, which were functionally important, have been identified in the promoter region of *GH3* in maize (D. Zhang *et al.*, 2016). By comparing the sequences of these *cis*-elements in the parental lines, differences in ASF1MOTIFCAMV (TGACG) were detected. There was one copy in Si-287, but two copies were found in Si-144. Amongst them, one copy, both in Si-287 and Si-144, was located at −857 bp (857 bp upstream of the 5'UTR region), another copy which existed only in Si-144, was located at −1288 bp (1288 bp upstream of the 5'UTR region), and there existed a 211 bp deletion in Si-287. We then designated the corresponding alleles as $Stg7^{Si\text{-}287}$ type (senescent allele) and $Stg7^{Si\text{-}144}$ type (stay-green or non-senescent allele), respectively (Fig. 5E). In-depth investigation of these allelic differences will facilitate understanding of the regulatory mechanisms of leaf senescence.

Population genetics of the effects of Stg3 *and* Stg7 *on leaf senescence and yield*

To further analyse the functions of the vital alleles in *ZmATG18b* and *ZmGH3.8*, we detected the natural allelic variations of these sites in a total of 173 maize inbred lines (Supplementary Table S1). Intriguingly, we found that according to the variations identified, genotypes of these inbred lines can be classified into four combinations, including $Stg3^{Si\text{-}144}/Stg7^{Si\text{-}144}$ type (n=51), $Stg3^{Si\text{-}144}/Stg7^{Si\text{-}287}$ type (n=98), $Stg3^{Si\text{-}287}/Stg7^{Si\text{-}144}$ type (n=5), and $Stg3^{Si\text{-}287}/Stg7^{Si\text{-}287}$ type (n=19) (Fig. 6A, B). Statistically, lines with $Stg3^{Si\text{-}144}/Stg7^{Si\text{-}144}$ type had a significantly (P<0.01) delayed leaf senescence (stay-green) phenotype than those with $Stg3^{Si\text{-}287}/Stg7^{Si\text{-}287}$ type. For lines with $Stg3^{Si\text{-}144}/Stg7^{Si\text{-}287}$ type and $Stg3^{Si\text{-}287}/Stg7^{Si\text{-}144}$ type, there were no significant differences (P>0.05) compared with $Stg3^{Si\text{-}144}/Stg7^{Si\text{-}144}$ type or $Stg3^{Si\text{-}287}/Stg7^{Si\text{-}287}$ type (Fig. 6B). In addition, we compared the ear weight of lines with different combinations of the $Stg3^{Si\text{-}144}$ and $Stg7^{Si\text{-}144}$ alleles and similar trends were observed (Fig. 6C). These results suggest that the stacking of $Stg3^{Si\text{-}144}$ and $Stg7^{Si\text{-}144}$ alleles could delay leaf senescence and increase ear weight in maize.

Additionally, we also explored the implications of identified alleles on maize breeding. We used Si-144 as the donor parent and NILs as the receptor parent for cross combination. The improved hybrids and Jidan27 were planted under two conditions: normal condition and drought stress condition. At 45 DAA, we calculated the ratio of green leaves of the improved hybrids and Jidan27 in the field. Compared with normal growth condition, the percentage of green leaves ratio reduction and ear weight loss traits in NIL-$Stg3^{Si\text{-}144}/Stg7^{Si\text{-}144}$ × Si-144 ($Stg3^{Si\text{-}144}/Stg7^{Si\text{-}144}$) were both significantly (P < 0.05) lower than that of Jidan27 under drought stress (Fig. 6D, E). Considering the two putative genes obtained and the performance of the stacking combination in inbred lines or improved hybrids, we suggested that the stacking effect might be controlled by the interaction between autophagy and auxin pathways.

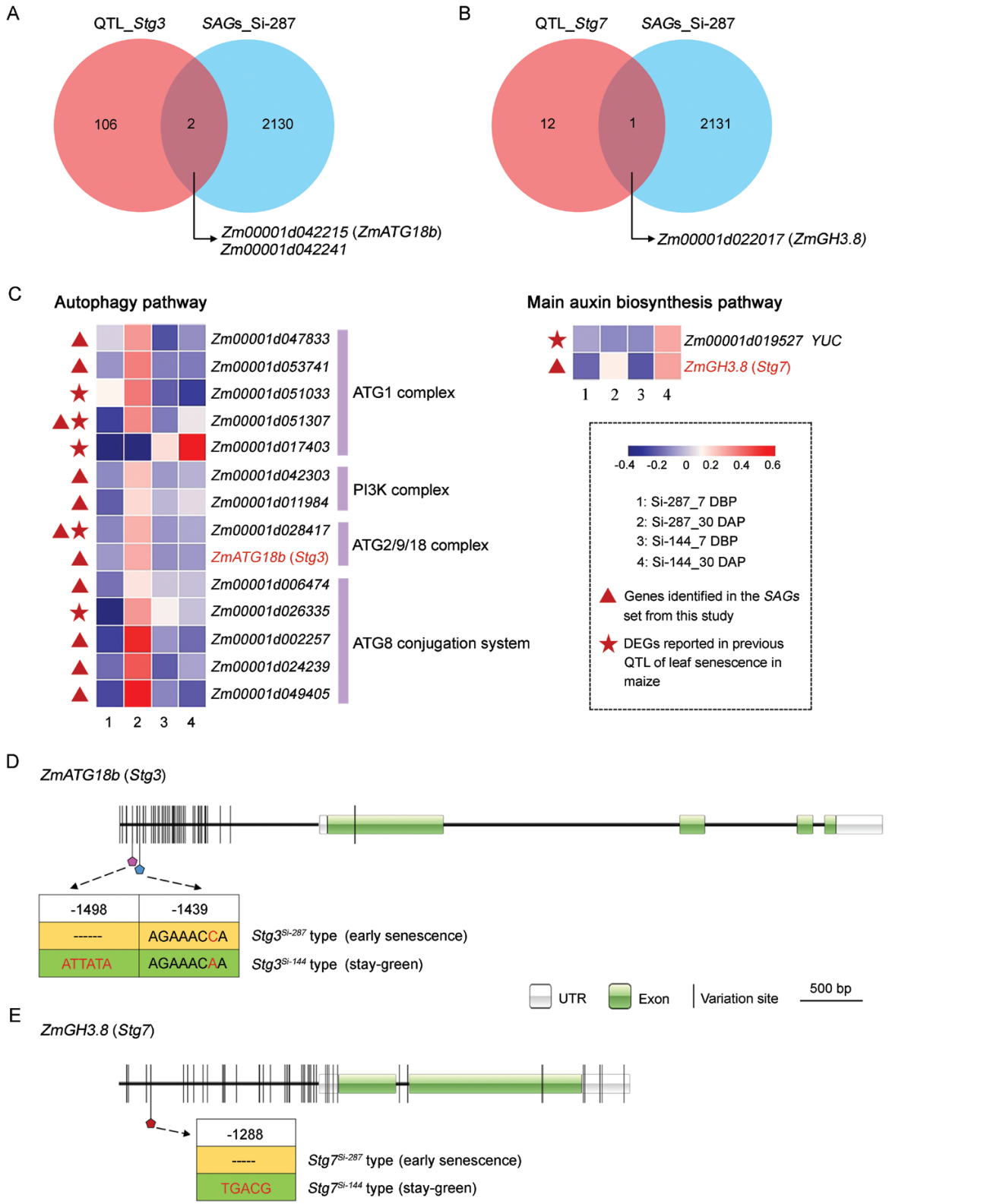

Fig. 5. Candidate genes revealed by the integrated analysis of QTL mapping and transcriptome analysis. (A) Candidate genes obtained from the comparison between genes in the locus of *Stg3* and *SAGs* set. *Zm00001d042215* and *Zm00001d042241* were the common genes identified. (B) Candidate genes obtained from the comparison between genes in the locus of *Stg7* and *SAGs* set. *Zm00001d022017* was the common gene obtained. (C) Genes in *SAGs* set or DEGs in the reported leaf senescence QTL which are involved in autophagy and the main auxin biosynthesis pathways. Boxes

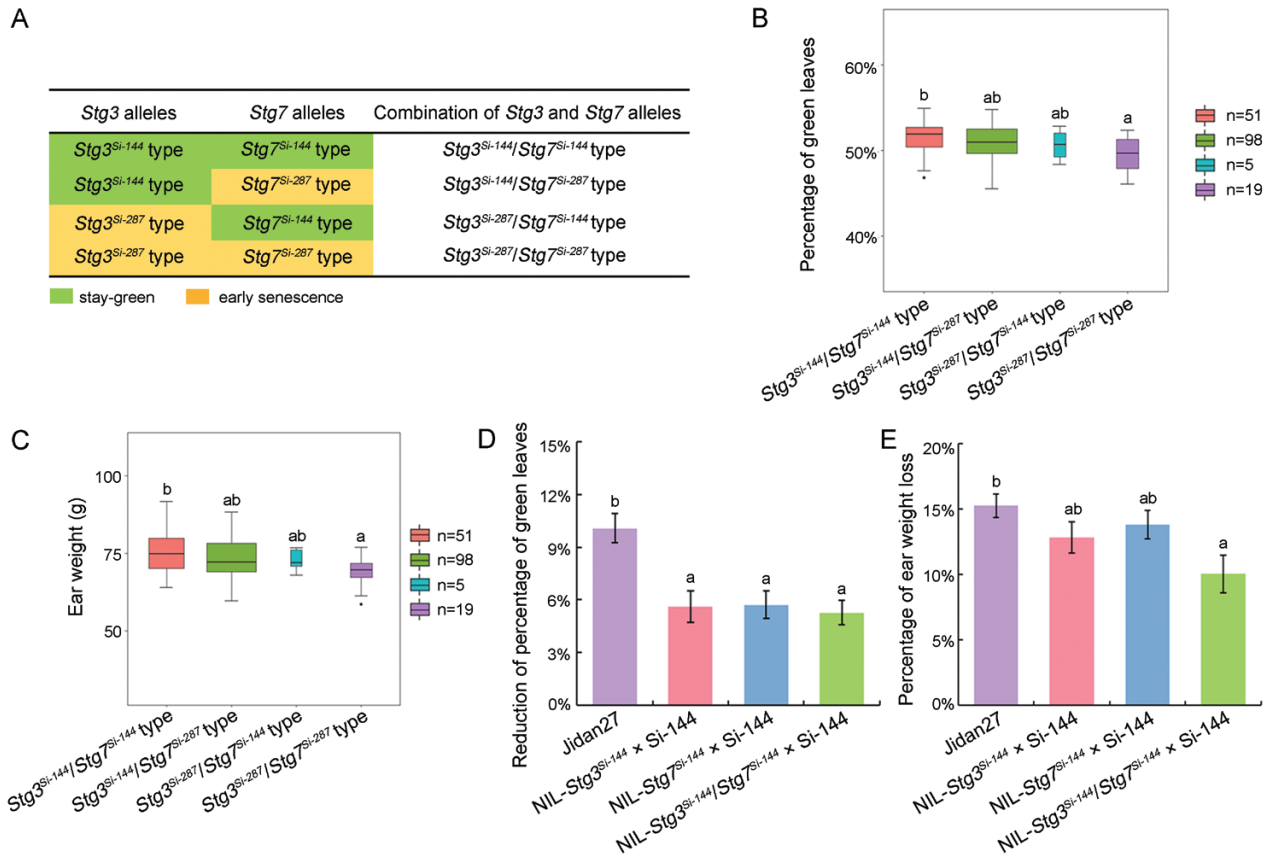

Fig. 6. Population genetics of the effect of *Stg3* and *Stg7* on leaf senescence and yield. (A) Four combinations of the obtained alleles in maize inbred lines. (B, C) Differences in leaf senescence phenotype (B), and ear weight (C) of the four combinations of *Stg3* and *Stg7* alleles. n denotes the number of genotypes belonging to each group. (D, E) Reduction of percentage of green leaves (D) and percentage of ear weight loss (E) of Jidan27 and improved hybrids under drought condition compared with water condition at 45 DAA. Data in (D) and (E) were obtained from at least eight plants of each kind, and values are the means ±SE. Letters above the columns represent differences at the 0.05 significance level determined by one-way ANOVA.

Fine-tuning interaction between Stg3 *and* Stg7 *on leaf senescence*

To further validate the function of the stacking effect of *ZmATG18b* and *ZmGH3.8*, we analysed the expression patterns of these two genes in the NILs and Si-287 at seven DBA and 30 DAA (Fig. 7A, B). Compared with seven DBA, *ZmATG18b* showed a down-regulation (negative fold-change) at 30 DAA in all the NILs, but it was up-regulated (positive fold-change) in Si-287. For *ZmGH3.8*, it was up-regulated (positive fold-change) in all the NILs and Si-287, while its expression in NIL-$Stg3^{Si\text{-}144}/Stg7^{Si\text{-}144}$ and NIL-$Stg7^{Si\text{-}144}$ were significantly higher (P<0.01) than that in NIL-$Stg3^{Si\text{-}144}$ and Si-287 at 30 DAA. Combining the leaf senescence phenotype of these lines, we found that down-regulation of *ZmATG18b* and up-regulation of *ZmGH3.8* was a favourable combination in delaying leaf senescence. It should be noted that the expression of *ZmATG18b* was the lowest at 30 DAA compared with other three lines (NIL-$Stg3^{Si\text{-}144}$, NIL-$Stg7^{Si\text{-}144}$ and Si-287), while that of *ZmGH3.8* was relatively moderate (higher than that in NIL-$Stg3^{Si\text{-}144}$ and Si-287, and lower than that in NIL-$Stg7^{Si\text{-}144}$) in NIL-$Stg3^{Si\text{-}144}/Stg7^{Si\text{-}144}$ at 30 DAA, which suggests that a subtle balance between the expression of these two genes is needed in NIL-$Stg3^{Si\text{-}144}/Stg7^{Si\text{-}144}$, leading to the delay of leaf senescence.

Considering the combination of $Stg3^{Si\text{-}144}/Stg7^{Si\text{-}144}$ and $Stg3^{Si\text{-}287}/Stg7^{Si\text{-}287}$ type lines exhibited significant differences

with different colours represent expression of each gene. The red triangles represent *SAG*s identified in this study, and the red asterisks represent DEGs in the reported leaf senescence QTL in maize. *YUC*, Yucca; *ATG*, Autophagy; PI3K, Phosphatidylinositol 3-kinase. (D, E) Schematic representation of the structure and sequence variations of *ZmATG18b* (D) and *ZmGH3.8* (E). The white boxes represent UTR regions, and the green boxes represent exons. The upstream region of the 5'UTR indicates the promoter region. The vertical black lines indicate variations between Si-287 and Si-144. The pentagons represent variation sites in the major *cis*-elements, different colours indicate different cis-elements. Variations of the marked sites between Si-287 and Si-144 were displayed with yellow and green background, respectively. $Stg3^{Si\text{-}287}$ type and $Stg7^{Si\text{-}287}$ indicate alleles of *ZmATG18b* and *ZmGH3.8* in Si-287, respectively. $Stg3^{Si\text{-}144}$ type and $Stg7^{Si\text{-}144}$ type indicate alleles of *ZmATG18b* and *ZmGH3.8* in Si-144, respectively.

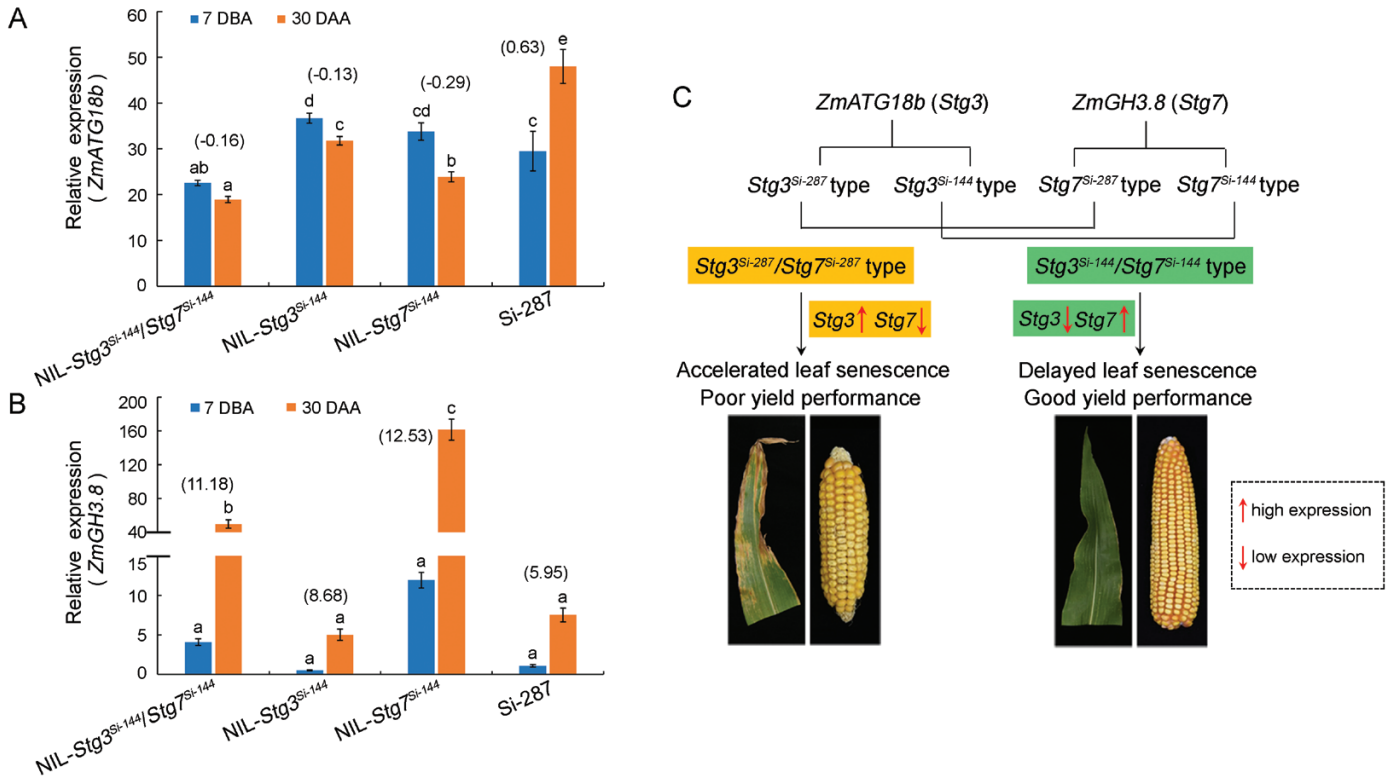

Fig. 7. Expression patterns of the candidate genes in different allelic combinations, and a proposed working model of *Stg3* and *Stg7* during leaf senescence. (A, B) Expression patterns of *ZmATG18b* (A) and *ZmGH3.8* (B) in different allelic combinations. Different letters above the histograms indicate differences at the 0.05 significance level determined by one-way ANOVA. Different numbers above the histograms indicate fold-change in expression at 30 DAA compared with seven DBA, and numbers below/above zero represent down-/up-regulation of gene expression. (C) A potential working model of *Stg3* and *Stg7* in leaf senescence. There are two alleles in *ZmATG18b* ($Stg3^{Si-144}$ and $Stg3^{Si-287}$ alleles) and *ZmGH3.8* ($Stg7^{Si-144}$ and $Stg7^{Si-287}$ alleles). As mentioned above, the combination of $Stg3^{Si-144}/Stg7^{Si-144}$ type line exhibited delayed leaf senescence phenotype and increased yield, while lines with $Stg3^{Si-287}/Stg7^{Si-287}$ type showed accelerated leaf senescence phenotype and had low yield. The expression of *ZmATG18b* (*Stg3*) in $Stg3^{Si-287}/Stg7^{Si-287}$type line was higher than that in $Stg3^{Si-144}/Stg7^{Si-144}$ type line, and the expression of *ZmGH3.8* (*Stg7*) in $Stg3^{Si-144}/Stg7^{Si-144}$ type line was higher than that of $Stg3^{Si-287}/Stg7^{Si-287}$ type line. Thus, we propose that the interaction between autophagy and auxin pathways might explain the differences in maize leaf senescence phenotypes.

in senescence phenotypes and yield character, as well as differences in the expression patterns of *ZmATG18b* and *ZmGH3.8* (Fig. 7C), we inferred that the interaction between autophagy and auxin pathways might be the cause of these performances. However, the underlying mechanism remains to be ascertained.

Discussion

Identification of candidate genes involved in leaf senescence by integrated analysis of QTL mapping and transcriptome profiling

Although previous QTL mapping studies identified multiple loci associated with leaf senescence across the 10 chromosomes of maize (Zheng *et al.*, 2009; Almeida *et al.*, 2014; Belícuas *et al.*, 2014), the position of *Stg3* and *Stg7* identified in this study are not in those reported regions, suggesting that they are two novel loci for maize leaf senescence. In sorghum, four classical loci regulating leaf senescence were identified (Xu *et al.*, 2000). Interestingly, the collinearity loci of *Stg3* and *Stg7* identified in this study were close to *Stg1* and *Stg3* in sorghum, respectively, indicating that mechanistic similarities might exist between maize and sorghum (Supplementary Fig. S5). Moreover, the yield data of improved hybrids and Jidan27 further confirmed the tolerance function of these two loci to drought stress. Under drought stress, ear weight losses of stacked NIL-$Stg3^{Si-144}/Stg7^{Si-144}$ × Si-144 was significantly lower than that of Jidan27 (Fig. 6E). These results were consistent with previous reports that timely delaying of leaf senescence can facilitate yield homeostasis under stress conditions (Thomas and Ougham, 2014; Zhang *et al.*, 2019). Therefore, we speculate that these two QTL identified in this study not only play important roles in delaying leaf senescence, but also have potential effects on maize yield stability under drought stress.

QTL mapping and transcriptomic analysis are important approaches for detecting the essential pathways or genes controlling quantitative traits of interest. Through integrated analysis of these two methods, two candidate genes *ZmATG18b* and *ZmGH3.8* were identified, and they were included in the 1655 common genes identified in the *SAG*s set in a previous study (Sekhon *et al.*, 2019) and ours (Fig. 4C), indicating their

potential importance in the regulation of leaf senescence. It has been reported that *ZmATG18b* plays an essential role in plant development and stress responses (Klionsky and Ohsumi, 1999; Li *et al.*, 2015), and that *ZmGH3.8* is involved in rice morphogenesis and response to stress tolerance (Du *et al.*, 2012).

The potential function of the candidate genes in the regulation of leaf senescence in maize

Expression pattern analysis revealed that the expression of *ZmATG18b* was higher in Si-287 than in NIL-$Stg3^{Si\text{-}144}$ at 30 DAA (Fig. 7A) , suggesting that this gene might be a positive regulator of maize leaf senescence. It has been reported that autophagy can be activated during leaf aging, and that *ATG18* is involved in the formation of autophagosome in Arabidopsis (Wang and Schippers, 2019). Some studies have also shown that the increase of autophagic activity can promote leaf senescence and cell death (Avila-Ospina *et al.*, 2014), suggesting the possibility of *ZmATG18b* in controlling maize leaf senescence. However, the underlying mechanism is still unclear.

Meanwhile, the expression of *ZmGH3.8* in NIL-$Stg7^{Si\text{-}144}$ was 20.4-fold higher than that in Si-287 at 30 DAA (Fig. 7B), suggesting its negative role in the regulation of maize leaf senescence. As *GH3* is involved in IAA (indole-3-acetic acid) conjugation (Staswick *et al.*, 2005), we speculated that changes in IAA concentration might be a main factor regulating leaf senescence. The role of auxin in leaf senescence is complex (Quirino *et al.*, 1999; van der Graaff *et al.*, 2006; Crane *et al.*, 2019), and the potential mechanism is still much less understood. Higher concentrations of free IAA were detected in the senescent line than in the non-senescent line (our ongoing work); further studies on auxin conjugation are needed to better understand the mechanisms.

Natural allelic variations of these two genes significantly contributed to leaf senescence phenotype and yield trait in maize, and better performance in both inbred lines with the optimal allelic combination and the improved stacking NILs than in Si-287/Jidan27 indicated the underlying interaction between *Stg3* and *Stg7*. However, the relevant mechanisms need to be studied further. Generally, reactive oxygen species (ROS) are a crucial component in plant responses to external stimuli (Gorlach *et al.*, 2015; Signorelli *et al.*, 2019). The accumulation of ROS can be influenced by auxin concentration and autophagic activity (Du *et al.*, 2012; Signorelli *et al.*, 2019). Further studies on the role of ROS in the connection between autophagy and auxin pathways in controlling leaf senescence are necessary.

In this study, four combinations were found for the natural allelic variations of *ZmATG18b* and *ZmGH3.8*. Lines with $Stg3^{Si\text{-}144}/Stg7^{Si\text{-}144}$ type showed higher green leaves ratio and increased ear weight compared with those of $Stg3^{Si\text{-}287}/Stg7^{Si\text{-}287}$ type. We questioned whether these combinations had been effectively used in maize breeding, so the elite inbred lines which have been widely used in hybrid maize breeding were examined. Amongst them, Qi-319 belongs to $Stg3^{Si\text{-}144}/Stg7^{Si\text{-}144}$ type, Zheng58, Huangzao4 and Ye478 are lines carrying $Stg3^{Si\text{-}144}/Stg7^{Si\text{-}287}$ type, and Chang7-2 is the line with $Stg3^{Si\text{-}287}/Stg7^{Si\text{-}144}$ type (Supplementary Table S1). As mentioned above, lines with $Stg3^{Si\text{-}144}/Stg7^{Si\text{-}287}$ and $Stg3^{Si\text{-}287}/Stg7^{Si\text{-}144}$ type displayed no significant differences in leaf senescence and yield traits compared with those in Si-287, hence improvement of lines with these two types into $Stg3^{Si\text{-}144}/Stg7^{Si\text{-}144}$ type would help the breeders to increase leaf stay-green rate and yield in maize.

Taken together, we identified two novel loci, *Stg3* and *Stg7,* controlling maize leaf senescence. Further analysis revealed that autophagy and auxin pathways might play crucial roles in leaf senescence at the transcriptional level. Natural allelic variations showed that the alleles of $Stg3^{Si\text{-}144}/Stg7^{Si\text{-}144}$ type, which could delay leaf senescence, is a favourable combination for increasing maize yield. In addition, the improved hybrids of NIL-$Stg3^{Si\text{-}144}/Stg7^{Si\text{-}144}$ × Si-144 exhibited lower yield loss under drought stress. The underlying mechanisms of *ZmATG18b* and *ZmGH3.8* in leaf senescence awaits further investigation.

Supplementary data

The following supplementary data are available at *JXB* online.

Fig. S1. Gene expression stability of the candidate reference genes calculated by NormFinder (A) and geNorm (B).

Fig. S2. Genetic composition of NIL-$Stg3^{Si\text{-}144}$ and NIL-$Stg7^{Si\text{-}144}$ on the chromosomes in maize.

Fig. S3. Senescence phenotypes of Si-287 and NILs.

Fig. S4. Candidate gene selection between *Zm00001d042215* and *Zm00001d042241* in *Stg3*.

Fig. S5. Collinearity of the two candidate loci *Stg3* and *Stg7* in maize and sorghum.

Table S1. Detailed information of maize inbred lines used in this study.

Table S2. Primers used for RT–qPCR analysis.

Table S3. The Minimum Information for Publication of Quantitative Real-Time PCR Experiments (MIQE) checklist.

Table S4. Molecular markers used for the identification of the candidate loci.

Table S5. Statistical analysis of filtered and mapped data of all samples in QTL-seq.

Table S6. Primers used for the amplification of candidate genes.

Table S7. QTL detected for leaf senescence in F_2 population.

Table S8. Detailed information of NILs (NIL-*Stg3Si-144*, NIL-*Stg7Si-144* and NIL-$Stg3^{Si\text{-}144}/Stg7^{Si\text{-}144}$) used in this study.

Table S9. Statistical analysis of RNA sequencing data of all samples.

Table S10. List of genes in the candidate region of *Stg3*.

Table S11. List of genes in the candidate region of *Stg7*.

Acknowledgements

We thank other members of Haichun Jing's lab for their assistance in this research. This work was supported by grants from the National Key Research and Development Plan of China (2016YFD0100605), the Ministry of Science and Technology of China (2018ZX08009-11B), and the Chinese Academy of Sciences (XDA24010106).

Conflict of interest

The authors declare no conflict of interest.

Author contributions

HCJ conceived and designed the experiments; XF and HQH performed the experiments; LLL, ZGL, and FS provided support for field phenotyping; XYW provided support for bioinformatics analysis; DYH provided support for materials; XF analysed the data and wrote the paper; HCJ and HQH revised the manuscript.

Data availability

The transcriptome raw data of Si-287 and Si-144 reported in this paper have been deposited in the Genome Sequence Archive (Wang *et al.*, 2017) in National Genomics Data Center, China National Center for Bioinformation, Chinese Academy of Sciences, under accession number CRA003926 that are publicly accessible at https://bigd.big.ac.cn/gsa. All other data supporting the findings of this study are available within the paper and within its supplementary data published online.

References

Almeida GD, Nair S, Borém A, Cairns J, Trachsel S, Ribaut JM, Bänziger M, Prasanna BM, Crossa J, Babu R. 2014. Molecular mapping across three populations reveals a QTL hotspot region on chromosome 3 for secondary traits associated with drought tolerance in tropical maize. Molecular Breeding **34**, 701–715.

Andersen CL, Jensen JL, Ørntoft TF. 2004. Normalization of real-time quantitative reverse transcription-PCR data: a model-based variance estimation approach to identify genes suited for normalization, applied to bladder and colon cancer data sets. Cancer Research **64**, 5245–5250.

Arnon DI. 1949. Copper enzymes in isolated chloroplasts. polyphenoloxidase in *Beta vulgaris*. Plant Physiology **24**, 1–15.

Avila-Ospina L, Moison M, Yoshimoto K, Masclaux-Daubresse C. 2014. Autophagy, plant senescence, and nutrient recycling. Journal of Experimental Botany **65**, 3799-3811.

Beavis WD, Smith OS, Grant D, Fincher R. 1994. Identification of quantitative trait loci using a small sample of topcrossed and F_4 progeny from maize. Crop Science **34**, 882–896.

Belícuas PR, Aguiar AM, Bento DAV, Câmara TMM, de Souza Junior CL. 2014. Inheritance of the stay-green trait in tropical maize. Euphytica **198**, 163–173.

Bertels J, Huybrechts M, Hendrix S, Bervoets L, Cuypers A, Beemster GTS. 2020. Cadmium inhibits cell cycle progression and specifically accumulates in the maize leaf meristem. Journal of Experimental Botany **71**, 6418–6428.

Bleecker AB, Patterson SE. 1997. Last exit: senescence, abscission, and meristem arrest in *Arabidopsis*. The Plant Cell **9**, 1169–1179.

Bresson J, Bieker S, Riester L, Doll J, Zentgraf U. 2018. A guideline for leaf senescence analyses: from quantification to physiological and molecular investigations. Journal of Experimental Botany **69**, 769–786.

Bustin SA, Benes V, Garson JA, *et al.* 2009. The MIQE guidelines: minimum information for publication of quantitative real-time PCR experiments. Clinical Chemistry **55**, 611–622.

Causse MA, Fulton TM, Cho YG, Ahn SN, Chunwongse J, Wu K, Xiao J, Yu Z, Ronald PC, Harrington SE. 1994. Saturated molecular map of the rice genome based on an interspecific backcross population. Genetics **138**, 1251–1274.

Chai M, Guo Z, Shi X, Li Y, Tang J, Zhang Z. 2019. Dissecting the regulatory network of leaf premature senescence in maize (*Zea mays* L.) using transcriptome analysis of *ZmELS5* mutant. Genes **10**, 944–961.

Christopher JT, Manschadi AM, Hammer GL, Borrell AK. 2008. Developmental and physiological traits associated with high yield and stay-green phenotype in wheat. Australian Journal of Agricultural Research **59**, 354–364.

Crane RA, Cardénas Valdez M, Castaneda N, Jackson CL, Riley CJ, Mostafa I, Kong W, Chhajed S, Chen S, Brusslan JA. 2019. Negative regulation of age-related developmental leaf senescence by the IAOx Pathway, PEN1, and PEN3. Frontiers in Plant Science **10**, 1202.

Du H, Wu N, Fu J, Wang S, Li X, Xiao J, Xiong L. 2012. A *GH3* family member, *OsGH3-2*, modulates auxin and abscisic acid levels and differentially affects drought and cold tolerance in rice. Journal of Experimental Botany **63**, 6467–6480.

Görlach A, Bertram K, Hudecova S, Krizanova O. 2015. Calcium and ROS: A mutual interplay. Redox Biology **6**, 260–271.

Gregersen PL, Culetic A, Boschian L, Krupinska K. 2013. Plant senescence and crop productivity. Plant Molecular Biology **82**, 603–622.

Guo Y, Gan SS. 2012. Convergence and divergence in gene expression profiles induced by leaf senescence and 27 senescence-promoting hormonal, pathological and environmental stress treatments. Plant, Cell & Environment **35**, 644–655.

Jing HC, Hille J, Dijkwel RR. 2003. Ageing in plants: conserved strategies and novel pathways. Plant Biology **5**, 455–464.

Jordan DR, Hunt CH, Cruickshank AW, Borrell AK, Henzell RG. 2012. The relationship between the stay-green trait and grain yield in elite sorghum hybrids grown in a range of environments. Crop Science **52**, 1153–1161.

Khanal R, Navabi A, Lukens L. 2015. Linkage map construction and quantitative trait loci (QTL) mapping using intermated vs. selfed recombinant inbred maize line (*Zea mays* L.). Canadian Journal of Plant Science **95**, 1133–1144.

Kim D, Langmead B, Salzberg SL. 2015. HISAT: a fast spliced aligner with low memory requirements. Nature Methods **12**, 357–360.

Klionsky DJ, Ohsumi Y. 1999. Vacuolar import of proteins and organelles from the cytoplasm. Annual Review of Cell and Developmental Biology **15**, 1–32.

Li F, Chung T, Pennington JG, Federico ML, Kaeppler HF, Kaeppler SM, Otegui MS, Vierstra RD. 2015. Autophagic recycling plays a central role in maize nitrogen remobilization. The Plant Cell **27**, 1389–1408.

Li B, Dewey CN. 2011. RSEM: accurate transcript quantification from RNA-Seq data with or without a reference genome. BMC Bioinformatics **12**, 323.

Liang C, Wang Y, Zhu Y, *et al.* 2014. *OsNAP* connects abscisic acid and leaf senescence by fine-tuning abscisic acid biosynthesis and directly targeting senescence-associated genes in rice. Proceedings of the National Academy of Sciences, USA **111**, 10013–10018.

Lin F, Jiang L, Liu Y, Lv Y, Dai H, Zhao H. 2014. Genome-wide identification of housekeeping genes in maize. Plant Molecular Biology **86**, 543–554.

Liu W, Xie Y, Ma J, *et al.* 2015. IBS: an illustrator for the presentation and visualization of biological sequences. Bioinformatics **31**, 3359–3361.

Liu X, Yuan Y, Martinez C, Babu R, Suarez EA, Zhang X, Neiff N, Trachsel S. 2020. Identification of QTL for early vigor and leaf senescence

across two tropical maize doubled haploid populations under nitrogen deficient conditions. Euphytica **216**, 42–55.

Livak KJ, Schmittgen TD. 2001. Analysis of relative gene expression data using real-time quantitative PCR and the 2(-Delta C(T)) Method. Methods **25**, 402–408.

Love MI, Huber W, Anders S. 2014. Moderated estimation of fold change and dispersion for RNA-seq data with DESeq2. Genome Biology **15**, 550.

Lu H, Lin T, Klein J, Wang S, Qi J, Zhou Q, Sun J, Zhang Z, Weng Y, Huang S. 2014. QTL-seq identifies an early flowering QTL located near *Flowering Locus* T in cucumber. Theoretical and Applied Genetics **127**, 1491–1499.

Mao C, Lu S, Lv B, Zhang B, Shen J, He J, Luo L, Xi D, Chen X, Ming F. 2017. A Rice NAC transcription factor promotes leaf senescence via ABA Biosynthesis. Plant Physiology **174**, 1747–1763.

Maxwell K, Johnson GN. 2000. Chlorophyll fluorescence–a practical guide. Journal of Experimental Botany **51**, 659–668.

Meng L, Li H, Zhang L, Wang J. 2015. QTL IciMapping: integrated software for genetic linkage map construction and quantitative trait locus mapping in biparental populations. The Crop Journal **3**, 269–283.

Messmer R, Fracheboud Y, Bänziger M, Stamp P, Ribaut JM. 2011. Drought stress and tropical maize: QTLs for leaf greenness, plant senescence, and root capacitance. Field Crops Research **124**, 93–103.

Murray MG, Thompson WF. 1980. Rapid isolation of high molecular weight plant DNA. Nucleic Acids Research **8**, 4321–4325.

Quirino BF, Normanly J, Amasino RM. 1999. Diverse range of gene activity during *Arabidopsis thaliana* leaf senescence includes pathogen-independent induction of defense-related genes. Plant Molecular Biology **40**, 267–278.

Schippers JH. 2015. Transcriptional networks in leaf senescence. Current Opinion in Plant Biology **27**, 77–83.

Schippers JH, Schmidt R, Wagstaff C, Jing HC. 2015. Living to die and dying to live: the survival strategy behind leaf senescence. Plant Physiology **169**, 914–930.

Sekhon RS, Childs KL, Santoro N, Foster CE, Buell CR, de Leon N, Kaeppler SM. 2012. Transcriptional and metabolic analysis of senescence induced by preventing pollination in maize. Plant Physiology **159**, 1730–1744.

Sekhon RS, Saski C, Kumar R, *et al.* 2019. Integrated genome-scale analysis identifies novel genes and networks underlying senescence in maize. The Plant Cell **31**, 1968–1989.

Signorelli S, Tarkowski ŁP, Van den Ende W, Bassham DC. 2019. Linking autophagy to abiotic and biotic stress responses. Trends in Plant Science **24**, 413–430.

Staswick PE, Serban B, Rowe M, Tiryaki I, Maldonado MT, Maldonado MC, Suza W. 2005. Characterization of an Arabidopsis enzyme family that conjugates amino acids to indole-3-acetic acid. The Plant Cell **17**, 616-627.

Takagi H, Abe A, Yoshida K, *et al.* 2013. QTL-seq: rapid mapping of quantitative trait loci in rice by whole genome resequencing of DNA from two bulked populations. The Plant Journal **74**, 174–183.

Thomas H, Ougham H. 2014. The stay-green trait. Journal of Experimental Botany **65**, 3889–3900.

Trachsel S, Sun D, SanVicente FM, Zheng H, Atlin GN, Suarez EA, Babu R, Zhang X. 2016. Identification of QTL for early vigor and stay-green conferring tolerance to drought in two connected advanced backcross populations in tropical maize (*Zea mays* L.). PLoS One **11**, e0149636.

Üstün S, Hafrén A, Hofius D. 2017. Autophagy as a mediator of life and death in plants. Current Opinion in Plant Biology **40**, 122–130.

van der Graaff E, Schwacke R, Schneider A, Desimone M, Flügge UI, Kunze R. 2006. Transcription analysis of Arabidopsis membrane transporters and hormone pathways during developmental and induced leaf senescence. Plant Physiology **141**, 776–792.

Vandesompele J, De Preter K, Pattyn F, Poppe B, Van Roy N, De Paepe A, Speleman F. 2002. Accurate normalization of real-time quantitative RT-PCR data by geometric averaging of multiple internal control genes. Genome Biology **3**, Research0034.1-0034.11.

Wang J, Guan H, Dong R, Liu C, Liu Q, Liu T, Wang L, He C. 2019. Overexpression of maize sucrose non-fermenting-1-related protein kinase 1 genes, *ZmSnRK1s*, causes alteration in carbon metabolism and leaf senescence in *Arabidopsis thaliana*. Gene **691**, 34–44.

Wang A, Li Y, Zhang C. 2012. QTL mapping for stay-green in maize (*Zea mays*). Canadian Journal of Plant Science **92**, 249–256.

Wang H and Schippers JHM. 2019. The role and regulation of autophagy and the proteasome during aging and senescence in plants. Genes 10, 267-289.

Wang Y, Song F, Zhu J, *et al*., 2017. GSA: Genome Sequence Archive. Genomics Proteomics Bioinformatics 15, 14-18.

Wu XY, Kuai BK, Jia JZ, Jing HC. 2012. Regulation of leaf senescence and crop genetic improvement. Journal of Integrative Plant Biology **54**, 936–952.

Xu W, Subudhi PK, Crasta OR, Rosenow DT, Mullet JE, Nguyen HT. 2000. Molecular mapping of QTLs conferring stay-green in grain sorghum (*Sorghum bicolor* L. Moench). Genome **43**, 461–469.

Yang Z, Li X, Zhang N, Wang X, Zhang Y, Ding Y, Kuai B, Huang X, Tuberosa R. 2017. Mapping and validation of the quantitative trait loci for leaf stay-green-associated parameters in maize. Plant Breeding **136**, 188–196.

Yang Z, Wang CQ, Qiu K, Chen HR, Li ZP, Li X, Song JB, Wang XL, Gao J, Kuai BK, Zhou X. 2020. The transcription factor *ZmNAC126* accelerates leaf senescence downstream of the ethylene signaling pathway in maize. Plant, Cell & Environment **43**, 2287–2300.

Yolcu S, Li X, Li S, Kim YJ. 2018. Beyond the genetic code in leaf senescence. Journal of Experimental Botany **69**, 801–810.

Young TE, Meeley RB, Gallie DR. 2004. ACC synthase expression regulates leaf performance and drought tolerance in maize. The Plant Journal **40**, 813–825.

Yu T, Lu X, Bai Y, Mei X, Guo Z, Liu C, Cai Y. 2019. Overexpression of the maize transcription factor *ZmVQ52* accelerates leaf senescence in *Arabidopsis*. PLoS One **14**, e0221949.

Zhang J, Fengler KA, Van Hemert JL, *et al.* 2019. Identification and characterization of a novel stay-green QTL that increases yield in maize. Plant Biotechnology Journal **17**, 2272–2285.

Zhang Z, Shang H, Shi Y, *et al.* 2016. Construction of a high-density genetic map by specific locus amplified fragment sequencing (SLAF-seq) and its application to Quantitative Trait Loci (QTL) analysis for boll weight in upland cotton (*Gossypium hirsutum*.). BMC Plant Biology **16**, 79.

Zhang WY, Xu YC, Li WL, Yang L, Yue X, Zhang XS, Zhao XY. 2014. Transcriptional analyses of natural leaf senescence in maize. PLoS One **9**, e115617.

Zhang D, Zhang N, Zhong T, Wang C, Xu M, Ye J. 2016. Identification and characterization of the *GH3* gene family in maize. Journal of Integrative Agriculture **15**, 249–261.

Zheng HJ, Wu AZ, Zheng CC, Wang YF, Cai R, Shen XF, Xu RR, Liu P, Kong LJ, Dong ST. 2009. QTL mapping of maize (*Zea mays*) stay-green traits and their relationship to yield. Plant Breeding **128**, 54–62.

Zheng M, Yang T, Liu X, *et al.* 2020. *qRf8-1*, a novel QTL for the fertility restoration of maize CMS-C identified by QTL-seq. G3 **10**, 2457–2464.